This is a repository copy of *Single particle flame-combustion studies on solid biomass fuels*.

Article:

Single particle flame-combustion studies on solid biomass fuels

*P.E. Mason[1], L.I. Darvell[1], J.M. Jones[1], M. Pourkashanian[2], A. Williams[2]

[1]Energy Research Institute, School of Chemical and Process Engineering (SCAPE), University of Leeds, Leeds, LS2 9JT, UK

[2]Energy Technology and Innovation Institute, SCAPE, University of Leeds, Leeds, LS2 9JT, UK

* Corresponding author - Email: pmpem@leeds.ac.uk - Telephone: +44 113 343 2498

Abstract

Combustion of solid biomass in large scale power generation has been recognized as a key technology for the transition to a decarbonized electricity sector in the UK by 2050. Much of the near-term forecast capacity is likely to be by the conversion of existing coal-fired pulverized fuel plant [1]. In such applications, it will be necessary to ensure that the combustion behaviour of the solid biomass fuels is engineered to match, as far as practical, that of the original plant design. While biomass feedstock characteristics vary considerably, one controllable variable for pulverized fuel is the size of the particles. Useful modelling for adaptation and design of boiler plant can be improved with more detailed measurement of the real behaviour of individual particles of the varying fuels. Typical power plant biomass fuels including pine, eucalyptus and willow with particle sizes ranging from up to 3mm [2] and with differing moisture content and aspect ratios were selected for study. Single particles were supported in a water-cooled cover and then exposed above a flame, simulating biomass combustion in a furnace. Measurements of ignition delay, volatile burning time and char burn-out time were undertaken using high speed image capture. Temperatures of the surrounding environment and near to the particle surface were measured with thermocouples and thermometric imaging. Thermo-gravimetric measurements on

separate samples complement the single particle measurements as a means of verifying the demarcation between the different stages of combustion and providing kinetic data.

Analysis of the data identified correlations between the biomass fundamental characteristics, particle size, and the observed combustion profiles. Empirical expressions for the duration of each combustion stage have been derived. These have been validated with basic modelling including the predicted devolatilisation stage calculated by the FG-Biomass model [3].

---

1. Introduction

Use of biomass as a fuel for electricity generation has, up until recent years, been a rather marginal application and the preserve of small scale installations. With the pressures of EU requirements to reduce nitrogen oxide pollution [4] and increasing political weight behind greenhouse gas emission controls, biomass has become a fuel choice for some of the largest power generation plant in Europe. It is likely that more conversions and perhaps new dedicated "flexi-fuel" conventional thermal power stations will feature in many European states' energy policies. Indeed, the UK government 2012 bioenergy strategy recognises large scale power generation from biomass as being a key technology for the transition to a decarbonised electricity sector by 2050 [1]. By 2020, it is projected that the UK will have over 30 TWh of electricity generation derived from combustion of up to 16 million dry tonnes of biomass [5].

For over a decade, most biomass in large scale operations has been crudely inserted into the existing fuel handling stream of conventional coal-fired stations. This co-firing, at levels of 10% (by mass) or so has

been a relatively simple means of displacing some of the coal and associated pollutants without significant alteration to the mills or burners. However, 2013 saw the first 100% biomass-fired 645MWe unit at Drax coming on-line - an unprecedented scale for electrical power generation in the UK.

Plant of such scale (>0.4GWe) requires more than 1GW of thermal input. Furnaces in conventional coal power stations of this size favour the use of pulverised fuel burners, coal having a tendency to pulverise consistently and reliably. Biomass, on the other hand, is less disposed to fracture uniformly especially transverse to the fibre alignment of anisotropic cellulosic materials. Whereas coal can be broken-down to <100µm particle sizes without excessive effort, similar milling effort on woody biomass can result in a spread of particle sizes and shapes ranging up to 3mm or so [2]. Since most solid biomass fuels have around 80% volatile content and generally less than 20% "fixed carbon", the burning profile differs somewhat from that of coal. Biomass combustion in furnaces designed for pulverised coal therefore needs careful consideration to ensure effective operation. The volatile combustion stage will tend to produce more rapid release of fuel energy in the early part of the furnace [6]. Larger particles can extend the period of heat release in this stage but the remaining char will also have an extended burn-out time, this can be at the expense of a high proportion of un-burned char passing through to the ash [7] or particles dropping out of suspension unburned in the furnace. Achieving a good balance between milling effort, heat release profile and char burn-out is therefore one of the main challenges for efficient use of biomass in conventional plant. Particle size and shape is therefore a key variable to be controlled so understanding the effects of particle size for various biomass is important.

In order to model and predict the combustion behaviour of pulverised biomass in large scale furnaces, some have taken a fundamental approach whereby the combustion of a single particle is used as a sub-

model (e.g. [8]). This approach requires the model of the single particle combustion to be refined before meaningful larger scale combustion can be extrapolated. The fundamental approach also requires good knowledge of the physical and chemical characteristics of the material such as thermal conductivity, heat capacity, porosity and kinetic parameters for pyrolysis and char combustion. Few, if any of these are known precisely for any given biomass fuel and there is a general paucity of experimental data to draw upon for refining and verifying such modelling.

Yang et al. [8] developed a computational model including heat transfer, mass transfer and chemical kinetics for cylindrical shaped particles in the range 0.5 – 20mm. While this compared favourably to experimental data presented for a single particle burning in entrained gas flow, a more robust validation would require more extensive experimentally derived data to be produced, covering the range of particle sizes. Other useful single particle modelling approaches have been set out by Haseli et al. [9] and Saastamoinen et al. [10].

Experiments on single particles of biomass have practical limitations in replicating the conditions in a pulverised fuel (p.f.) furnace. However there have been a number of experimental methods documented which examine combustion behaviour of biomass particle dimensions in the order of 1mm [11-15]. These have investigated the influence of variables including particle size and shape, gas temperature and oxygen concentration with the intention of informing and validating models.

Flower and Gibbins [11] developed apparatus in which single particles of biomass were suspended on a wire mesh and heated to 900°C in less than 0.5 seconds using an electrical element radiant heater.

Experimental data for the drying, devolatilisation and char burn-out was obtained for European Ash wood with differing moisture contents.

Lu et al. [12] suspended single particles in an enclosed chamber reactor with a pre-heated air/nitrogen feed and internal heating elements enabling gas temperatures up to 1037°C. Using poplar wood and hardwood sawdust particles in the size range $0.3 - 9.5$mm, the experiment focussed on the effects of shape differences on devolatilisation times, demonstrating that shape and aspect ratio differences affect the heat transfer and thereby show measurable differences in pyrolysis rates. Lu and Baxter [13] proceeded to directly measure the internal thermal gradients produced in these conditions using thermocouples in the centre and surface of 11mm diameter particles. The data from this was used for validation of CFD modelling by Gubba et al. [14].

Momeni at al. [15, 16] developed experimental apparatus using a gas burner and mass flow controllers to control the temperature and oxygen concentration in a vertical tube reactor in which single particles were placed for observing the combustion behaviour. The experiment examined ignition, devolatilisation and char burn-out for cylindrical particles with similar mass (12.5mg) with aspect ratios ranging from 1 to 6 and for gas temperatures ranging from 1200°C to 1600°C (with oxygen concentrations ranging from 5 to 20% for the burn-out tests). Similar experiments performed by Riaza et al. [17] using a drop tube furnace and high speed camera on moving particles milled to <150μm, report burnout times for various biomass and oxygen concentrations.

While it is recognised that "biomass" fuel covers large variations, previous experiments have tended to examine only one or two materials with a relatively small number of data points. The time-consuming

5

and laborious nature of preparing and burning individual particles places a limit on the volume of data that can be easily extracted.

In this investigation, we present an experiment examining the correlations between particle mass and the combustion behaviour; in particular, the conversion times for each stage of combustion, namely: ignition delay; volatile flame duration and char burn duration. In order to identify correlations amidst the variability and measurement noise, a large sample set (>100) has been used for each material.

2. Method

2.1 Preparation of samples

Three different biomass materials were selected for comparison: Pine, Eucalyptus and Willow. For consistency, the particles selected from the woody materials were selected without bark or obvious knotty structure (i.e. apparent as clean white wood).

Each particle was trimmed to a roughly cuboid/cylindrical shape using a razor to dimensions in the range 0.5mm to 4mm. The dimensions in the 3 principal axes were measured using a handheld micrometer (+/- 0.01mm). Each particle was weighed on a microbalance (+/- 0.01 mg). Although the particle shapes were not precisely regular, a good estimate of the volume and surface area was obtained using the mean values calculated for a cuboid and cylinder with the same principal dimensions. The mean particle density for each material, as presented in table 1, was derived from these measurements. These mean values were used subsequently to derive from the particle mass, an equivalent spherical particle size in heat transfer calculations.

Small batches of particle samples were wetted by adding small amounts of deionised water and storing in a sealed container for >24 hours. These were weighed again just prior to combustion. The typical

delay between weighing and ignition was 90 seconds ensuring not more than 10% loss of moisture, the loss rate being verified by measurement of control samples. Moisture content is reported as the ratio (%) of mass of water to the total mass of the particle.

2.2 Combustion apparatus

To ensure a stable and consistent combustion environment, a Méker type natural gas burner was used. This produces a flame with a wide base and a stable and relatively uniform core. The temperature profile of the flame on a selected burner was measured using a type-R thermocouple with corrections for radiative heat loss accounted for. The central part of the flame was recorded to be at 1550°C +/- 25°C. The oxygen concentration at the centre of the flame was also measured using a gas-analyser probe and recorded to be a consistent 10.75% +/- 0.25%. The temperatures in large scale pulverized fuel furnaces are in a similar range and, while oxygen concentration varies depending on fuel/air mix and position in the flame, this is also not unrepresentative. An extension to the experiment may consider creating different oxygen conditions as has been achieved in others' experiments using alternative apparatus [15]. In the experiments performed in this work, the particles of fuel were supported on a fine steel needle, in turn supported in a ceramic tube fixed to a solid support frame. A moveable water-cooled sleeve running coaxially over the needle/ceramic tube allowed the fuel sample to be protected from the gas flame. When the video recording was underway, the water-cooled sleeve was rapidly withdrawn thus exposing the sample to the combustion environment in a moment which can be identified to within one frame of the high speed video in the post-analysis.

2.3 Video image

7

A *FujiFilm Finepix HS10* camera was used for video recording. In general, a recording speed of 120 frames per second was used to obtain a reasonable balance between timing accuracy and image quality. The post-analysis of the video images was performed using standard software which allows frame-by-frame viewing and counting (and therefore timing) and adjustment of the image contrast and brightness.

2.4 Characterisation of materials

Samples of each material were analysed to determine fundamental characteristics by means of proximate analysis, ultimate analysis (CHNO) and calorimetry in accordance with applicable European Standards [18-21]. Chemical kinetics characteristics were obtained by thermo-gravimetric analysis performed on samples milled to <90μm particle size using a TA Instruments Q5000 analyser. Kinetics parameters were derived assuming single step first-order Arrhenius reactions for both pyrolysis stage and char burn stage. The pyrolysis kinetic parameters are obtained from analysis of the first stage devolatilisation reaction since this will dominate at fast heating rates [22].

3. Results

3.1 Characteristics of materials

The proximate analyses, elemental composition and estimated Higher Heating Value (HHV) for the three materials studied are presented in Table 1. It can be observed that their volatile and fixed carbon contents are comparable. All samples have relatively low ash contents ≤2% and similar HHVs (~19-20 MJ kg^{-1}). Their moisture contents were <10%, with the willow sample being significantly dryer than the other two (2.8 %H$_2$O).

There were no major differences in their elemental composition, with the exception of their nitrogen contents, which ranged between 0.1-1.3%.

8

3.2 Drying and ignition

The time-interval between the withdrawal of the protective sleeve and the on-set of volatile combustion is taken to be the "ignition delay". The delay is governed by the time required for the moisture to evaporate from the particle and also for the particle to heat up and start devolatilisation sufficient to produce a visible volatile flame. While the early stages of devolatilisation are difficult to identify visually, a consistent criteria for defining the start of the volatile flame was taken to be the first frame in which strong luminance could be detected using 100% contrast filter on the video.

In many cases, the ignition delay was measured in the order of 10-20 frames which implies an error of +/- 10% in the timing. However, the imprecision of this particular measurement appears to be overshadowed by other factors which disturb the nature of the "drying" phase such as the tendency of smaller parts and protuberances of the particles to ignite before the main bulk thus recording shorter ignition times for some relatively large particles than smaller ones.

Figures 1 (a)-(c) show the ignition delay plotted against the particle dry mass for each material, both "as received" (<10% moisture) and with added moisture (>40% moisture). Despite the noisy data, there are certain trends and correlations that can be inferred. As would be expected, there is a discernible trend for larger particles to have longer ignition delay even though there is a good deal of scatter in the data. The plot for the ignition delay versus moisture content for all materials (Fig. 1 (d)) shows an expected general trend for ignition delay to be longer for higher moisture content.

3.3 Devolatilisation and volatile combustion

9

The criteria for determining the visible start of the volatile flame was described in the previous section. The end of the volatile flame was determined in a similar manner with the luminance of the visible flame being strongly demarcated by setting the video playback to maximum contrast. The end of the volatile flame is much more distinct and the margin of error for this measurement is no more than one or two frames (<1%) of the total duration. The volatile flame duration for both dry and wet particles was plotted against particle dry mass for each of the fuels and is presented in Figure 2. In this instance, over 100 data points were recorded for each fuel.

The plot of the volatile flame duration times for the particles with added moisture reveals that flame durations are longer with respect to dry mass of the particle. This is evidence of the catalytic effect of alkali metal content in the devolatilisation stages which has been described previously in Jones et al. [23] and Saddawi et al. [24]. Particles with added moisture were subjected to excess water in the wetting process which, unavoidably, dissolved and extracted a significant proportion of potassium salts from the solid.

3.4 Char combustion

In the entrained gas flow, the particles do not burn evenly since the leading edge of the particle in the flame is subject to a higher heat transfer than the trailing edge. One effect of this one-sided heating is that the bottom of the particle commences char combustion before the top part of the particle has completed devolatilisation. Demarcating the start of the char combustion stage is therefore difficult to define. For the purposes of the experiment, a consistent and well-defined criterion for identifying the start of char combustion is required and, for convenience, it is taken to be coincident with the end of the volatile flame burn. The end of char combustion is taken to be the end of the discernible luminescent

10

emission from the char combustion. Identifying the latter of these markers visually is not as precise since there is a long diminuendo in the luminescence of the char combustion. However, use of the video contrast and brightness controls was found to assist in identifying a consistent end point for measurement purposes.

The char burn duration plotted against particle dry mass for each of the fuels is presented in Figure 3. The data is less consistent than that for the volatile flame duration and this is attributed mainly to the difficulty in identifying a clear cut-off criteria. The plot of the char duration times for the particles with added moisture shows a small difference with the as received samples. There appears to be some variation showing longer burn times in the eucalyptus and willow but with few data points and with much noise on the timing measurement, a significant difference is difficult to infer. Similar marginal differences between raw and water-washed particles have been reported by Jones et al. [23] with the suggestion that the soluble metals are either lost during devolatilisation or are not as active in catalysing the char burn out stage as they are in the devolatilisation stage.

4. Discussion and analysis

The usefulness of the data presented above depends on whether meaningful relationships can be extracted from it which can be shown to be: a) predictive to a practical level and: b) consistent with theoretical explanations of the physical processes. Empirical expressions derived from the data to predict ignition delay, volatile burning duration and char burn duration will certainly be of practical use in the design of furnaces and fuel preparation (drying and milling criteria). The results show relationships between particle mass and burning times which, although not directly comparable owing to differing

11

operating temperature and oxygen content, are similar to those presented by Flower and Gibbins [11] which, having fewer data points and particles greater than 5mg, are approximated to linear functions.

4.1 Comparison of experimental data with modelling

4.1.1   Ignition Delay

As particles of fuel enter the furnace environment they are introduced into the established flame with a gas temperature in a similar range to that of the experiment (~1800K). Exposure to this environment is sudden, virtually a step change in temperature also in a similar manner to the experiment. In an idealised model, the particle will heat up in accordance with convective and radiative heat transfer mechanisms described by the equation:

$$\frac{dT_p}{dt} = \frac{A_p}{m_p C_p} \left[h\left(T_f - T_p\right) + \varepsilon_p \sigma (T_R^4 - T_p^4) \right] \qquad (1)$$

Where:

m_p is the mass of the particle

A_p is the surface area of the particle

C_p is the specific heat capacity of the particle

T_p is the temperature of the particle

T_f is the temperature of the flame

T_R is the temperature of the enclosing surface

ε_p is the emissivity of the particle surface

σ is the Stafan-Boltzman constant (5.67×10^{-8} W m^{-2} K^{-4})

12

h is the convective heat transfer coefficient for the particle in a moving hot gas stream

There are significant differences between the experiment and a p.f. furnace: the relative gas flow over the fixed particle in the experiment is around 3.0 m s^{-1} whereas the relative velocity of the gas to a freely moving particle in a furnace will be lower as the particle is carried in the flow; the radiative heat loss in the experiment is against an ambient surface temperature of ~300K whereas in a furnace, the heat transfer surfaces may be in excess of 800K.

An approximation for modelling the drying rate for small particles (~2mm) is given by Peters [25]. Adapting for the loss of moisture in terms of mass we can use the function given by equations:

$$\frac{dm_w}{dt} = (T_p - T_e)\left(\frac{m_w}{m_{w0}}\right)\frac{\rho_w V_p \, C_{pw}}{\Delta H} \qquad\qquad T_p \geq T_e \qquad\qquad (2a)$$

$$\frac{dm_w}{dt} = 0 \qquad\qquad\qquad\qquad\qquad T_p < T_e \qquad\qquad (2b)$$

Where:

m_w is the mass of moisture in the particle at time t

m_{w0} is the initial mass of moisture in the particle

ρ_w is the density of water (1000 kg m^{-1})

ΔH is enthalpy of vaporization of water (~2.26x10^6 J kg^{-1})

C_{pw} is the specific heat capacity of water (~4181 J kg^{-1} K^{-1})

V_p is the volume of the particle

T_e is the temperature above which, moisture evaporates from the particle (~373K)

13

Equation 1 can then be modified to include the mass and heat capacity of moisture and also the heat loss component associated with the loss of moisture: $dm_w.\Delta H$. These are accounted for in the heating-up model.

With a fluid velocity of 3.0ms^{-1}, the Reynolds number, Re for 1-4mm diameter (~1-12mg) particles range from 10-50. In this range, the Nusselt number, Nu may be approximated [26] by the expression:

$$Nu = 2 + (0.4Re^{\frac{1}{2}} + 0.06Re^{\frac{2}{3}})Pr^{0.4}\left(\frac{\mu}{\mu_s}\right)^{1/4} \tag{3}$$

Where:

$\frac{\mu}{\mu_s}$ is the ratio of fluid dynamic viscosities at the flame temperature and the particle surface temperature

Pr is the Prandtl number for the fluid (~ 0.71 as for air)

The heat transfer coefficient for the cold particle placed in the flame is calculated from:

$$h = \frac{Nu.\lambda_{ext}}{D} \tag{4}$$

Where:

λ_{ext} is the thermal conductivity of the hot gas (~0.12 W m^{-1} K^{-1} at 1800K)

D is the equivalent diameter of the particle (for a sphere with same volume as the particle and where the volume is derived from the particle mass and mean particle density)

Taking a flame temperature of 1800K (1527°C) as in the experiment, the heating rate and drying rate expressions can be evaluated over small discrete time steps to make an indicative model for the expected ignition delay. Emissivity of the particle is taken as 0.9 and ambient surface temperature is taken as 300K. Figure 4 (a) shows the effect of increasing moisture level on the heating rate of a 2x1x1mm (~1mg) particle based on this model.

This model is useful in deriving a simplified empirical relationship between particle size, moisture content and ignition delay. While there is no clear specific point on the heating curve where we can identify consistently that ignition will occur, there will be a relationship between the temperature of the particle and the moment at which ignition can be observed as a luminescent volatile flame. From thermo-gravimetric analysis, we can examine the onset temperature of devolatilisation, which starts at a very low rate; as low as 420K. By 500K the mass loss is proceeding at a significant rate, and the appearance of a visible volatile flame should be expected around this point. The time taken for the modelled particle to reach 500K may then be taken as an index to relate to ignition delay. Since the real particle is not uniform as in the idealised case, some parts of the particle may dry, heat up and devolatilise faster than other parts. It is noted that moisture loss continues to occur for a significant duration after the particle temperature is above 500K. Drying and devolatilisation will therefore be occurring simultaneously for part of the time in accordance with the drying and devolatilisation behaviour of 1mm scale particles reported by Thunman et al. [27].

From the model, the relationship between particle size and the 300-500K heating time is close to the function:

$$\tau_{300-500} = a.m_p{}^b \tag{5}$$

15

Where a and b are functions of the initial moisture content, M (where $M = \frac{m_w}{m_p + m_w}$). For the modelled

1mg particle in the example, the functions are approximated as linear giving four coefficients in the equations:

$$a = 6.2M + 0.16 \tag{6a}$$

$$b = 0.77M + 0.49 \tag{6b}$$

The heating up time modelled on this basis is shown for 3 different moisture levels in figure 5(a). The form of this function appears to correspond well with the ignition delay data so it is reasonable to base a model of ignition delay τ_{ign} on the same form with the function:

$$\tau_{ign} = a_{ign} m_p{}^{b_{ign}} \tag{7}$$

Where a_{ign} and b_{ign} are empirically derived coefficients.

Fitting the data from the single particle combustion experiments to a function of the same form using least squares regression, ignition delay should then be predicted as a function of mass and moisture.

The modelling coefficients can be derived from best-fitting to the experimental data with different moisture content. Based on the experimental data for the three different materials, modelling functions are presented in Table 2.

In the case of the willow data, the model functions for M=3% and M=50% are plotted in figure 5 (b) alongside the measured data for particles with similar moisture content. While there is much variation and noise in the data, the model is capable of indicating an expected average ignition delay for different moisture contents. The coefficients evaluated from the experimental data vary by factors up to 5 from

those derived from the simplified model in equations (6a) and (6b) since these were based on heating up times rather than actual ignition times.

4.1.2 Volatile flame duration

The form of the best-fit function to the measured data for the volatile flame duration τ_{vol} is:

$$\tau_{vol} = a_{vol}m_p{}^{b_{vol}} \tag{8}$$

Where a_{vol} and b_{vol} are empirically derived coefficients.

In order to determine if these coefficients can be consistently predicted as functions of the material characteristics, a model of the devolatilisation process is required. A simplified model of the volatile flame duration can be made on the basis of the initial volatile mass, rate of reaction and particle temperature.

We have already presented a model for the heating rate of the particle in terms of convective, radiative heat transfer and moisture evaporation. We make a definition that the start of devolatilisation is the point of "ignition" which, in the model above, has been taken to be coincident with a particle temperature of 500K even though there may have been a small amount of devolatilisation before the appearance of a volatile flame. The rate of devolatilisation may be modelled in a simplified form as a first-order, single step Arrhenius reaction [8] as:

$$\frac{dm_{vol}}{dt} = -m_v A_v e^{-\frac{E_v}{RT_p}} \tag{9}$$

Where:

m_{vol} is volatile mass content of the particle at time t

A_v and E_v are the reactivity pre-exponential coefficient and activation energy for devolatilisation respectively.

The form of the relationship between particle mass and devolatilisation time can be extracted from the model by selecting reference values of A_v and E_v and determining the time interval between the points at which the particle has 1% and 99% volatile mass for various sizes of particle. An index of the devolatilisation time can then be plotted against the particle dry mass.

Figure 6 (a) shows the effect on the devolatilisation times using this model on particles with kinetic parameters as measured for the pine sample (see table 1) and for particles with mass ranging from 0.5 to 8 mg. The particle heating profiles from the model were also applied to the FG-BioMass model [3] and devolatilisation times derived in a similar manner. It should be noted that the FG-BioMass model has been deemed accurate for very small particle sizes since it is based on intrinsic kinetics, and as such it does take into account any mass transfer or heat transfer limitations encountered in larger particles. Nevertheless, as a means to validate the devolatilisation model, it is a useful baseline. Figure 6(b) shows the calculated devolatilisation times from the FG-Biomass model alongside the equivalent best-fit function derived from the experimental data. The FG-Biomass devolatilisation modelling confirms the form of the relation between particle mass and devolatilisation time as being a power function. However, there is a discrepancy in scale of about a factor of 2. This can be accounted for by including a term of the internal heat transfer to the centre of the particle τ_{int}. The characteristic time for the internal heat transfer can be approximated using the expression for heat transfer in a spherical solid [28]. In terms of the particle size and its thermal properties this is given by:

$$\tau_{int} \approx 0.17 \frac{r^2 \rho C_p}{\lambda_{int}} \tag{10}$$

18

Where:

λ_{int} is the thermal conductivity of the solid particle ($\sim$0.14 W m^{-1} K^{-1})

C_p is the specific heat capacity of the solid particle ($\sim$1800 J kg^{-1} K^{-1})

ρ is the density of the particle ($\sim$480 kg m^{-3})

r is the particle radius (derived for a sphere with same volume as the particle)

By including this additional term proportional to the square of the radius, the devolatilisation time model can be extended. The resulting function, also plotted in figure 6(b), shows a good approximation to the experimental data and validates the use of the best fit function given in equation (8). Having established that the relation between particle mass and flame duration is power function consistent with simplified modelling, the experimental data can be fitted to a least-squares regression to determine the respective volatile flame duration model coefficients for each material. These are summarised in table 3.

4.1.3   Char burn-out duration

The data recorded for the duration of char-burn out with respect to particle dry mass is affected by measurement noise, mainly as a result of the indistinct visual signs indicating the end of the burning. Nevertheless, the large data set allows trends to be identified. The char burn duration is, for convenience, measured as starting from the end of the volatile flame. However, since the convective heat transfer is asymmetrical, with the leading side of the particle heating most quickly, there is overlapping between the volatile and char combustion stages. As char burn actually starts in the lower part of the particle before the upper part has completely devolatilised and the duration of the overlapping has been discounted in the measurements of char combustion, there is then a distortion between the

19

measured and actual char burn duration. Nevertheless, an analysis can be made of the measured data and an adjustment applied to obtain a consistent predictive model.

The char oxidation reaction may be modelled in a simplified form as a first-order, single step Arrhenius reaction [8]. At the start of the char burn, the particle is near to the maximum temperature that would be achieved through convective heat transfer alone. The heat of the char reaction adds to the particle temperature further so a continued temperature rise occurs. To simplify the analysis in the first instance, we can assume a fixed particle temperature and therefore a fixed rate of reaction. In such a case, for a given mass of char, the rate of mass loss would be an exponential decay with a characteristic time proportional to the mass. The time for the char to burn out in this model would then be a simple linear function of mass. Examination of the experimental data shows that a least squares linear regression function produces a reasonable fit ($R^2 > 0.7$). The char burn duration τ_{chr} can then be approximated by:

$$\tau_{chr} = a_{chr} m_p \tag{11}$$

Where a_{chr} is an empirically derived coefficient.

The coefficients for the three wood materials examined are given in Table 4. It is noted that there is a stronger divergence in the char burn duration between the three materials than for the volatile burn duration. This is reflected in the larger differences in the measured kinetics (see Table 1) for char burn. Indeed, there appears to be a simple correlation between the kinetic parameters for char combustion and the resulting char burn duration coefficient a_{chr}. Additional materials would need to be added to the data set to fully evaluate this correlation.

4.2 Analysis of other particle properties

20

4.2.1 Effects of particle density

The density of each particle could be estimated from the measured dimensions and mass of each particle. The density for particles of the same materials from the same samples was variable. Although some of this variability can be accounted for in the bands of error in measurement of volume (+/- 10%) and mass (+/-1%), the spread of density in each sample (+/- 1.96σ) was between 24 and 32% indicating that there is significant variability within the same material. The density was calculated on the dry mass basis for the samples of each material. Analysis of the data showed a close fit to a normal distribution. The curves based on the normal distribution parameters for each sample are shown in Figure 7.

For the different materials, a simple comparison of burning times with respect to density shows that there is no clear correlation. Eucalyptus, having a relatively high density (ρ=0.67 mg.mm^{-3}) has a somewhat slower volatile and char burn than willow with a lower density (ρ=0.52 mg.mm^{-3}). However, pine, with a density (ρ=0.48 mg.mm^{-3}) more similar to willow has a volatile and char burn duration closer to eucalyptus.

The volatile burn duration data for a single material can also be analysed with respect to density by dividing the data for each material into "higher density" (ρ>mean+0.5σ), "middle density" (mean-0.5σ<ρ<mean+0.5σ) and "lower density" (ρ<mean-0.5σ) fractions.

The results of this analysis for the Eucalyptus data are presented in Figure 8(a). Using the best fit regression line with the form of equation (8) for each fraction shows a discernible effect whereby the volatile burn duration is longer for higher density particles with equal mass. Analysis on the pine data showed a similar effect although the willow data was less discernible.

The char burn out data may be examined in a similar manner. As shown in figure 8(b), the char burn duration is plotted against the different density fractions of each material. The trend is similar to that of

the volatile flame data: the higher density particles have longer char burn duration. Modelling of pulverised fuel combustion should therefore take into account the spread of particle densities since this has a distinct effect.

4.2.2   Effects of Shape

Since the dimensions of each individual particle were recorded, the sample size allows some examination of the effects of shape on the volatile flame duration. The shape of a particle can be examined in a number of ways. Four shape types for convex particles can be classified using Zingg classification [29]. The shape types are based on the various aspect ratios of the 3-axes of the particle which are classified as: equant (ball), prolate (rod), oblate (disc) and bladed (strip). Figure 9 (a) shows a plot of the data which discriminates the four shape types. The differences are minor but trend lines show that bladed particles have a shorter volatile burn duration than equant.

The disparity of the dimensions of a shape, characterised by the "aspect ratio", can also be examined. The aspect ratio of each particle can be taken to be the ratio of the largest orthogonal dimension to the shortest orthogonal dimension. While all equant shapes have an aspect ratio of less than 2, prolate, oblate and bladed particles can all have large aspect ratios. Figure 9(b) shows a plot of the Willow data which discriminates four aspect ratio ranges (<2, 2-3, 3-4 and >4). In this analysis, there is a more discernible trend in the volatile flame duration characteristic time with respect to aspect ratio such that increased aspect ratio tends towards a quicker volatile burning time. The effect is expected since the heat transfer per unit of mass is greater, and consequently the devolatilisation time shorter, for higher aspect ratio particles - as confirmed in the findings of experiments by Momeni et al. [15] and in modelling investigations as reported by Gubba et al.[14].

22

While the effect of the orientation (with respect to the gas flame) of higher aspect ratio particles was also examined, the observed differences were marginal and not significant against other measurement noise.

5. Conclusions

An experimental method for examining the duration of the different stages of combustion of single particles has been presented and this has been applied to three woody biomass fuels. The volume of data has allowed the evaluation of empirical expressions for the relationship between particle mass and ignition delay, volatile flame duration and char burn duration. These empirical relationships have been reinforced by verification of the form of the functions by simple models of the principle physical processes. This approach can lead to a much simplified means of characterising fuel with regards the expected ignition delay, volatile combustion duration and char burn-out times. This means of characterisation may be used to inform modelling of combustion of pulverised biomass as well as being a means of validating existing models. Further detailed analysis has provided insight into the effects of the particle density and shape on the duration of the different stages of combustion.

Future work should aim to develop more consistent empirical "rules of thumb" for solid biomass fuel combustion characteristics correlated to readily measureable properties such as density. Furthermore, use of modelling together with analysis of single particle combustion behaviour may be used to infer less readily measureable properties such as thermal conductivity and heat transfer parameters. This can be achieved by extending the range of materials to include other varied woody biomass and also herbaceous materials.

Refining this technique to characterise fuels, in a timely manner, in terms of the measured duration of various stages of combustion would provide a useful tool to predict burn-out behaviour for varying particle size. This could then inform operators with regards to adjusting milling requirements to achieve optimum particle size distributions for the furnaces."

23

References

[1] DECC, UK Bioenergy Strategy, in: D.o.E.C. Change (Ed.), 2012.

[2] S. Van Loo, J. Koppejan, The handbook of biomass combustion and co-firing, Earthscan, 2008.

[3] Y. Chen, S. Charpenay, A. Jensen, M.A. Wójtowicz, M.A. Serio, Modeling of biomass pyrolysis kinetics, Symposium (International) on Combustion, 27 (1998) 1327-1334.

[4] EU, Directive 2001/80/EC - on the limitation of emissions of certain pollutants into the air from large combustion plants, in, ec.europa.eu, The European Parliament and the Council of the European Union, 2001, pp. 21.

[5] A.L. Stephenson, D.J.C. Mackay, Life Cycle Impacts of Biomass Electricity in 2020, in, Department of Energy and Climate Change, 2014.

[6] S.R. Gubba, D.B. Ingham, K.J. Larsen, L. Ma, M. Pourkashanian, H.Z. Tan, A. Williams, H. Zhou, Numerical modelling of the co-firing of pulverised coal and straw in a 300 MWe tangentially fired boiler, Fuel Processing Technology, 104 (2012) 181-188.

[7] D. Gera, M.P. Mathur, M.C. Freeman, A. Robinson, Effect of large aspect ratio of biomass particles on carbon burnout in a utility boiler, Energy & Fuels, 16 (2002) 1523-1532.

[8] Y.B. Yang, V.N. Sharifi, J. Swithenbank, L. Ma, L.I. Darvell, J.M. Jones, M. Pourkashanian, A. Williams, Combustion of a single particle of biomass, Energy & Fuels, 22 (2008) 306-316.

[9] Y. Haseli, J.A. van Oijen, L.P.H. de Goey, A detailed one-dimensional model of combustion of a woody biomass particle, Bioresource Technology, 102 (2011) 9772-9782.

[10] J. Saastamoinen, M. Aho, A. Moilanen, L.H. Sørensen, S. Clausen, M. Berg, Burnout of pulverized biomass particles in large scale boiler – Single particle model approach, Biomass and Bioenergy, 34 (2010) 728-736.

[11] M. Flower, J. Gibbins, A radiant heating wire mesh single-particle biomass combustion apparatus, Fuel, 88 (2009) 2418-2427.

[12] H. Lu, E. Ip, J. Scott, P. Foster, M. Vickers, L.L. Baxter, Effects of particle shape and size on devolatilization of biomass particle, Fuel, 89 (2010) 1156-1168.

[13] H. Lu, L.L. Baxter, Biomass Combustion Characteristics and Implications for Renewable Energy, in: P. Grammelis (Ed.) Solid Biofuels for Energy: a Lower Greenhouse Gas Alternative, Springer, 2011, pp. 95-121.

[14] S.R. Gubba, L. Ma, M. Pourkashanian, A. Williams, Influence of particle shape and internal thermal gradients of biomass particles on pulverised coal/biomass co-fired flames, Fuel Processing Technology, 92 (2011) 2185-2195.

[15] M. Momeni, C. Yin, S.K. Kær, T.B. Hansen, P.A. Jensen, P. Glarborg, Experimental Study on Effects of Particle Shape and Operating Conditions on Combustion Characteristics of Single Biomass Particles, Energy & Fuels, 27 (2012) 507-514.

[16] M. Momeni, C. Yin, S. Knudsen Kær, S.L. Hvid, Comprehensive Study of Ignition and Combustion of Single Wooden Particles, Energy & Fuels, 27 (2013) 1061-1072.

[17] J. Riaza, R. Khatami, Y.A. Levendis, L. Álvarez, M.V. Gil, C. Pevida, F. Rubiera, J.J. Pis, Combustion of single biomass particles in air and in oxy-fuel conditions, Biomass and Bioenergy, 64 (2014) 162-174.

[18] C.E.N. Standard, BS EN 15148:2009 Solid biofuels - Determination of the content of volatile matter, in, BSI, 2009.

[19] C.E.N. Standard, BS EN 14775:2009 Solid biofuels - Determination of ash content, in, BSI, 2009.

[20] C.E.N. Standard, BS EN 14918:2009 Solid Biofuels - Determination of calorific value, in, BSI, 2009.

[21] C.E.N. Standard, BS EN 15104:2011 Solid biofuels - Determination of total content of carbon, hydrogen and nitrogen - Instrumental methods, in, BSI, 2011.

[22] A. Saddawi, J.M. Jones, A. Williams, M.A. Wojtowicz, Kinetics of the Thermal Decomposition of Biomass, Energy & Fuels, 24 (2010) 1274-1282.

[23] J.M. Jones, L.I. Darvell, T.G. Bridgeman, M. Pourkashanian, A. Williams, An investigation of the thermal and catalytic behaviour of potassium in biomass combustion, Proceedings of the Combustion Institute, 31 (2007) 1955-1963.

[24] A. Saddawi, J.M. Jones, A. Williams, Influence of alkali metals on the kinetics of the thermal decomposition of biomass, Fuel Processing Technology, 104 (2012) 189-197.

[25] B. Peters, Thermal conversion of solid fuels, WIT Press, 2003.

[26] F.P. Incropera, D.P. DeWitt, Fundamentals of heat and mass transfer, 4th ed., Wiley, 1986.

[27] H. Thunman, K. Davidsson, B. Leckner, Separation of drying and devolatilization during conversion of solid fuels, Combustion and Flame, 137 (2004) 242-250.

[28] A.N. Hayhurst, The kinetics of the pyrolysis or devolatilisation of sewage sludge and other solid fuels, Combustion and Flame, 160 (2013) 138-144.

[29] T. Zingg, Beitrag zur Schotteranalyse, in, ETH Zurich, Zurich, 1935.

26

TABLES

Table 1 - Characteristics and kinetic parameters of biomass samples

Parameters	Basis	Units	Pine	Eucalyptus	Willow
Moisture content	as received	%wt	8.3	8.1	2.8
Ash content	dry	%wt	2.0	0.9	1.9
Volatile content	daf	%wt	82.5	83.3	83.6
Fixed carbon	daf	%wt	17.5	16.7	16.4
HHV	dry	MJ.kg^{-1}	18.6	19.4	19.8
Elemental					
C	daf	%wt	47.4	49.2	50.8
H	daf	%wt	5.3	5.6	6.0
O	daf	%wt	45.9	45.1	42.7
N	daf	%wt	1.3	0.1	0.4
Mean particle density	dry	mg.mm^{-3}	0.48	0.67	0.52
Pyrolysis kinetics					
Pre-exponential, A		s^{-1}	32900	1100	3170
Activation energy, E_a		kJ.mol^{-1}	72	56	65
Char burnout kinetics					
Pre-exponential, A		s^{-1}	1.27E+05	9.20E+05	672
Activation energy, E_a		kJ.mol^{-1}	94	113	70

Table 2 - Coefficients for the calculation of ignition delay.

	Pine	Eucalyptus	Willow
Ignition delay $\quad \tau_{ign} = a_{ign} m_p{}^{b_{ign}}$			
a_{ign}	$1.3M$	$1.4M$	$1.5M + 0.05$
b_{ign}	$0.4M + 0.32$	$0.3M + 0.37$	$0.4M + 0.25$

Table 3 - Coefficients for the calculation of volatile flame duration.

	Pine	Eucalyptus	Willow
Volatile flame duration $\quad \tau_{vol} = a_{vol} m_p{}^{b_{vol}}$			
a_{vol}	1.33	1.27	1.17
b_{vol}	0.59	0.62	0.60
R^2	0.98	0.94	0.93

Table 4 - Coefficients for the calculation of char combustion duration.

	Pine	Eucalyptus	Willow
Char burn duration $\quad \tau_{chr} = a_{chr} m_p$			
a_{chr}	2.52	2.90	2.02
R^2	0.80	0.72	0.86

FIGURES

Figure 1 – ignition delay versus particle dry mass for: (a) pine; (b) eucalyptus; (c) willow; (d) ignition delay versus moisture content for all samples.

Fig 1A
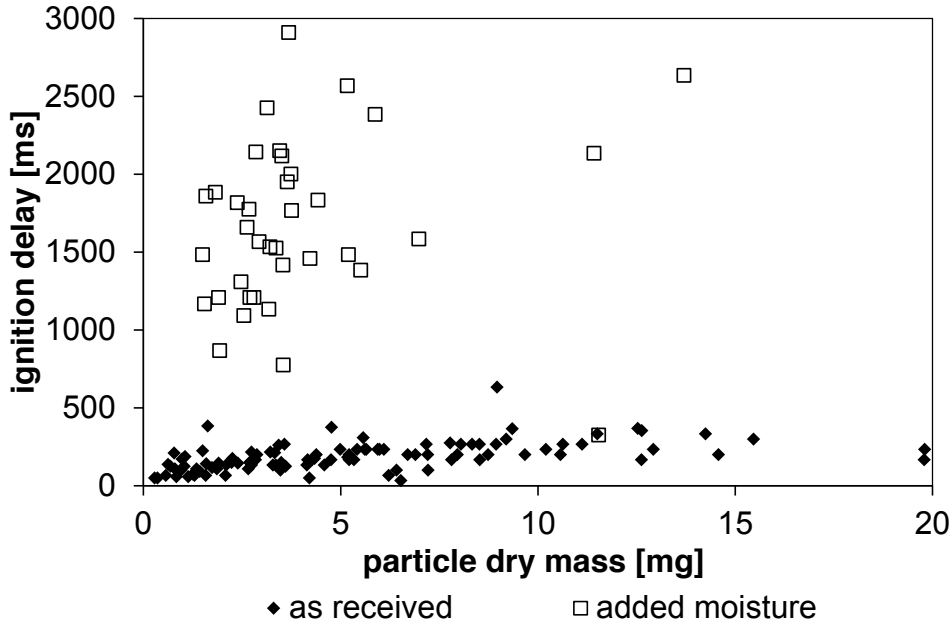
Fig 1B
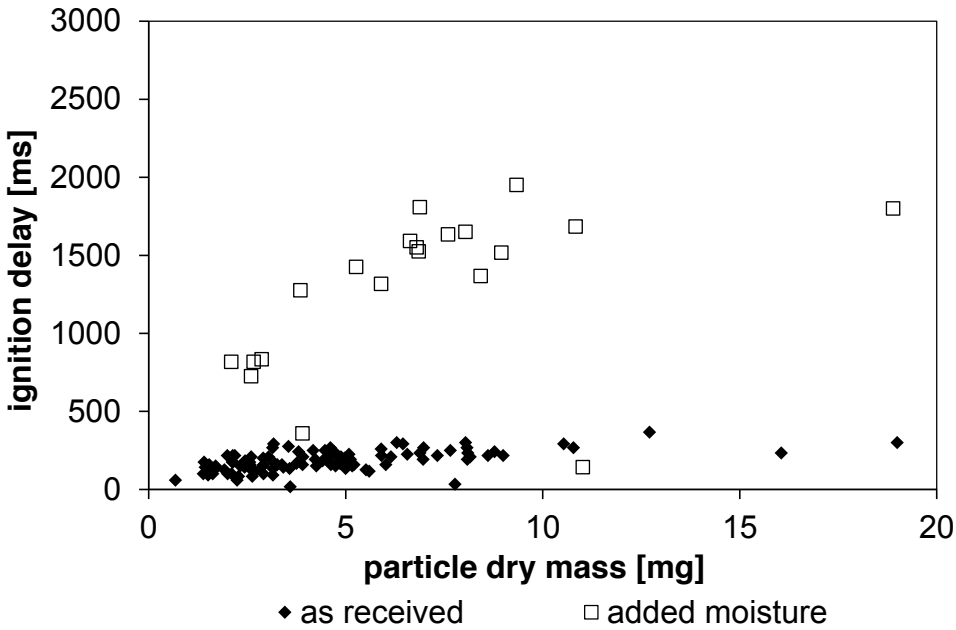
Fig 1C
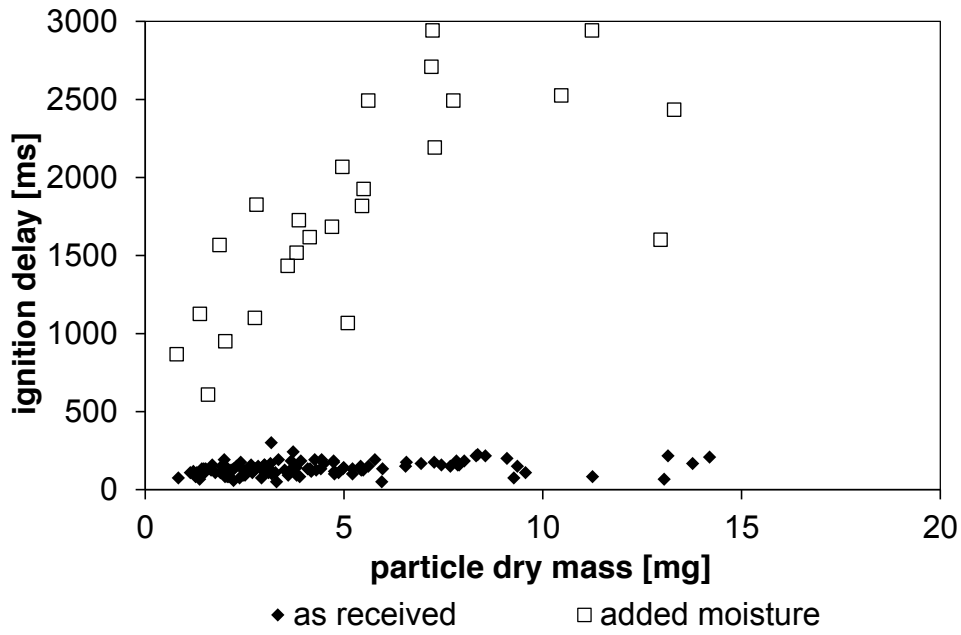
Fig 1D
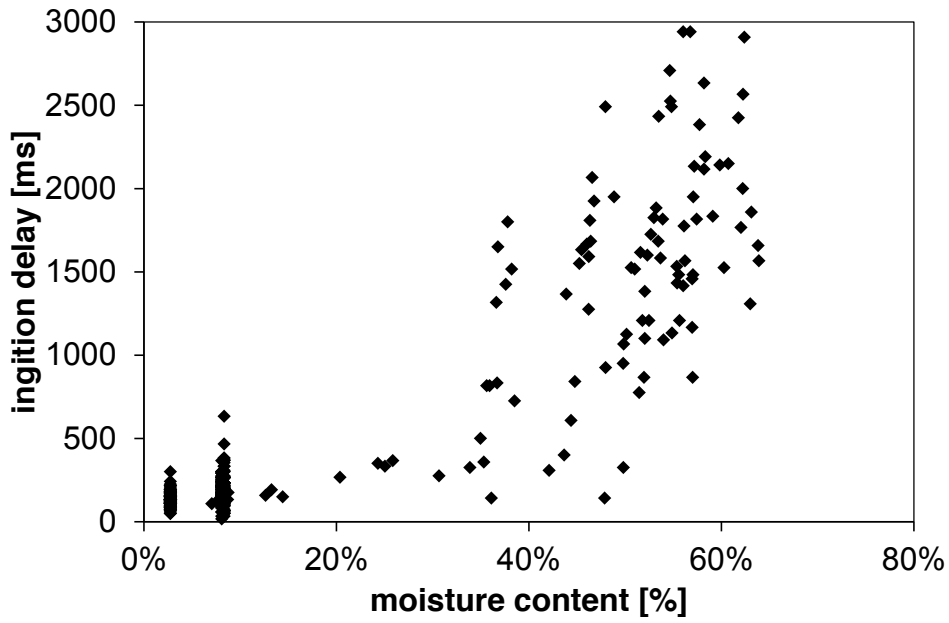
Figure 2 – Volatile flame duration versus dry particle mass for samples as received and with added moisture: (a) pine; (b) eucalyptus; (c) willow.

Fig 2A
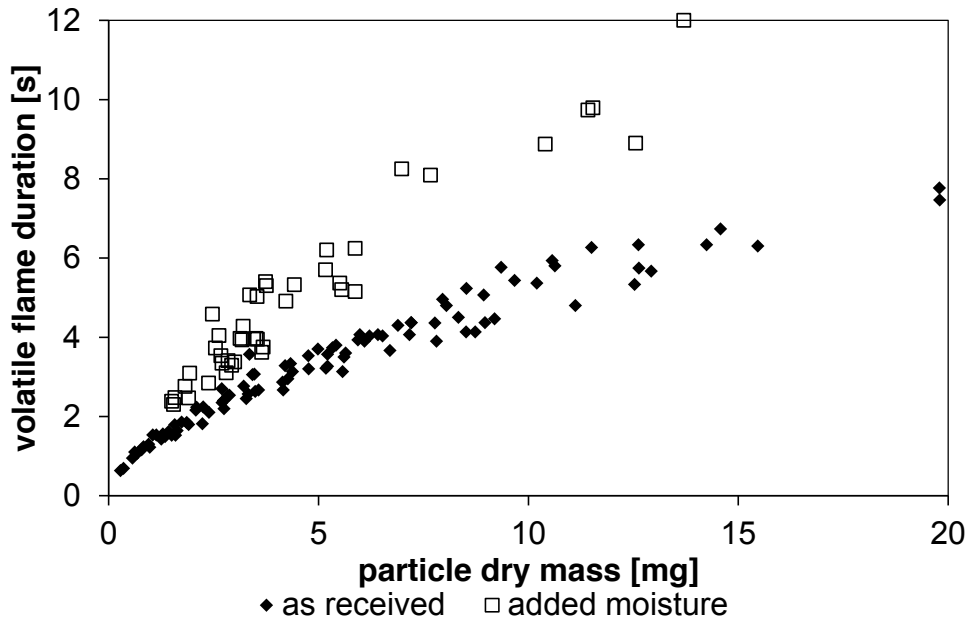
Fig 2B
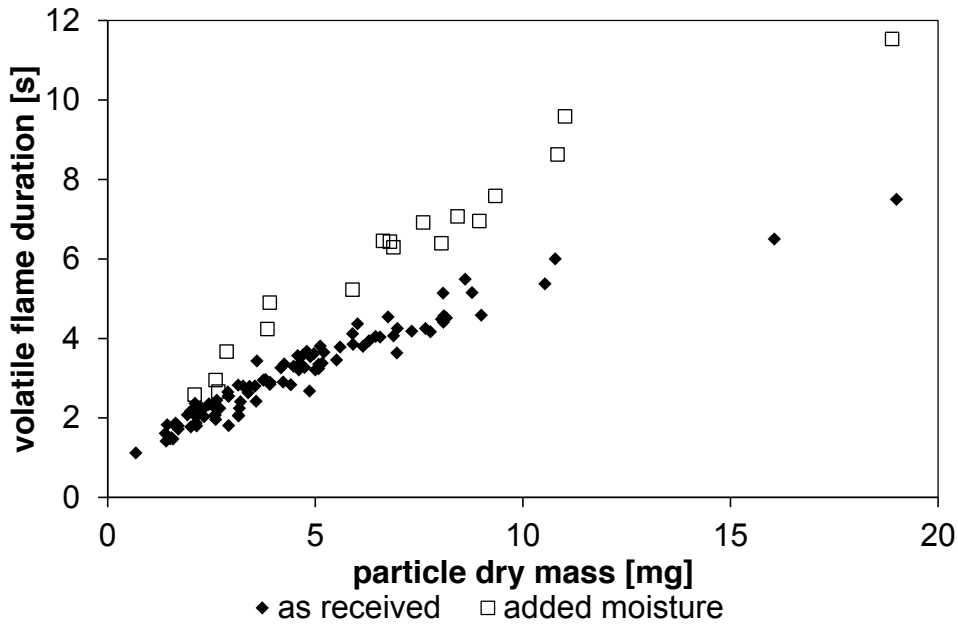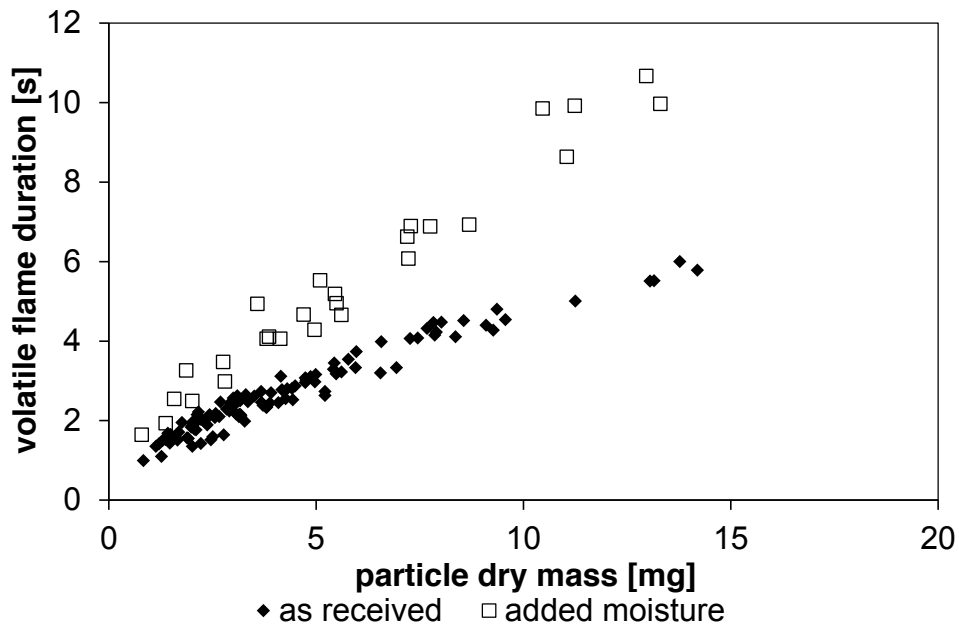
Figure 3 – Char burn duration versus dry particle mass for samples as received and with added moisture: (a) pine; (b) eucalyptus; (c) willow.

Fig 3A
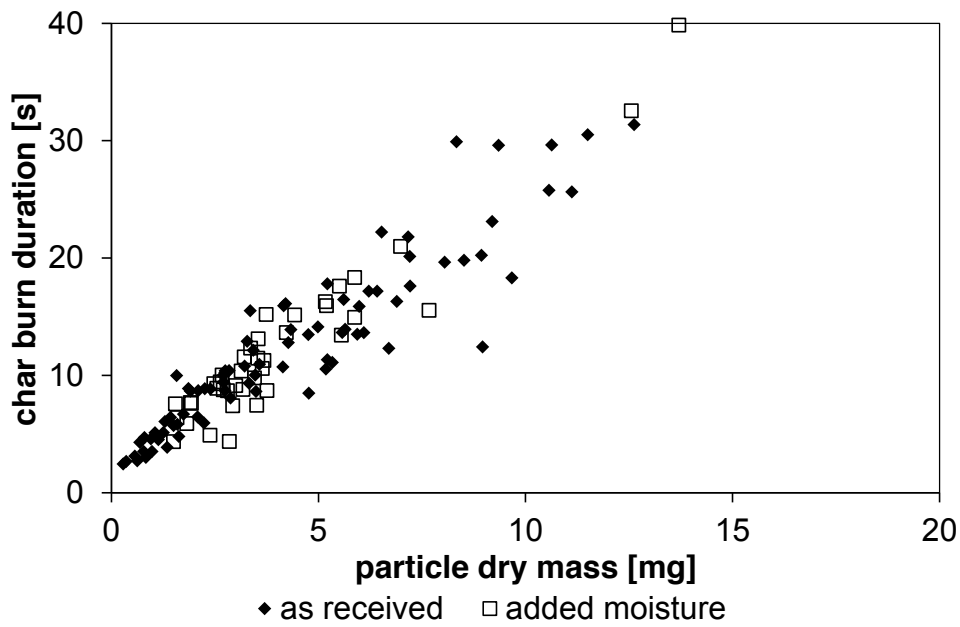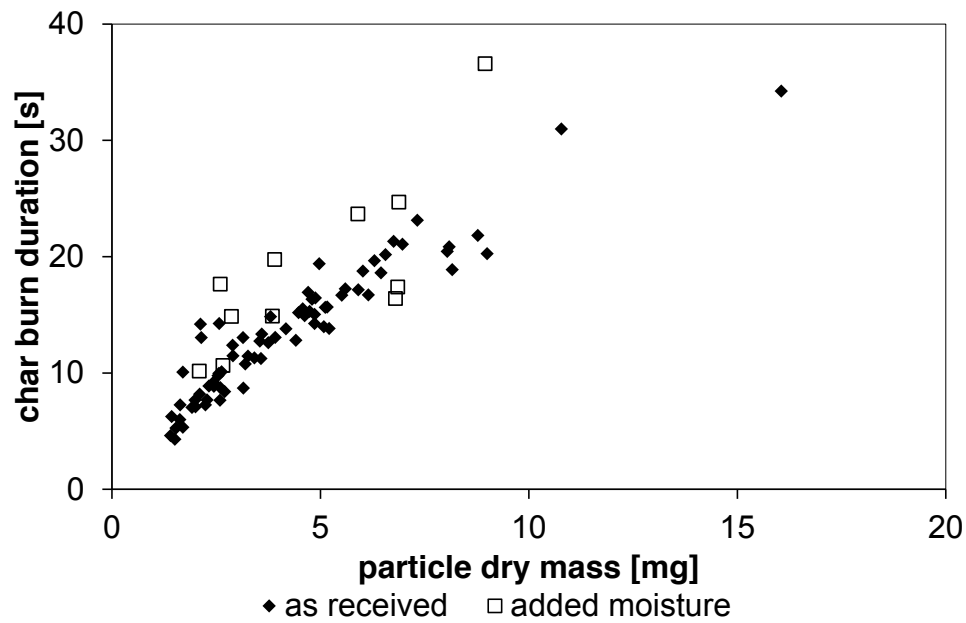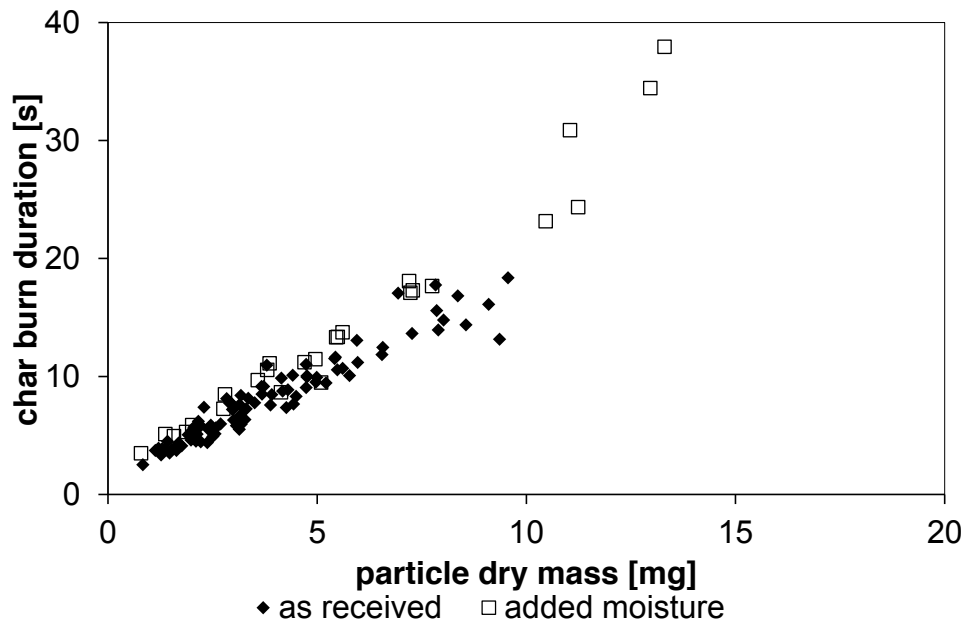
Figure 4 – initial heating rate of a wood particle: (a) modelled with respect to initial moisture content; (b) as measured using thermometric imaging of particle surface, M=40%, m=10mg; (c) modelled with respect to particle size.

Fig 4A
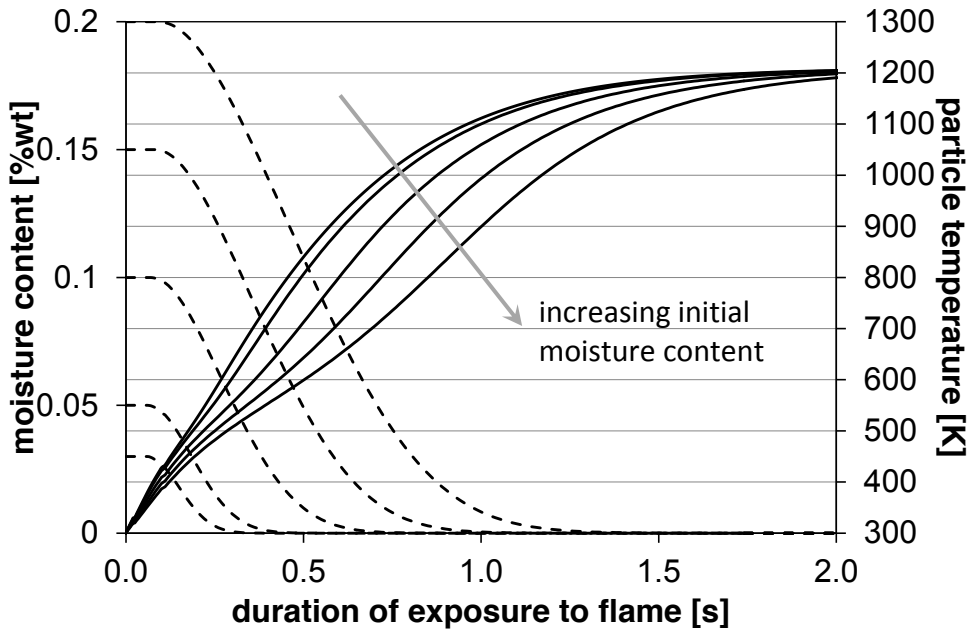
Fig 4B
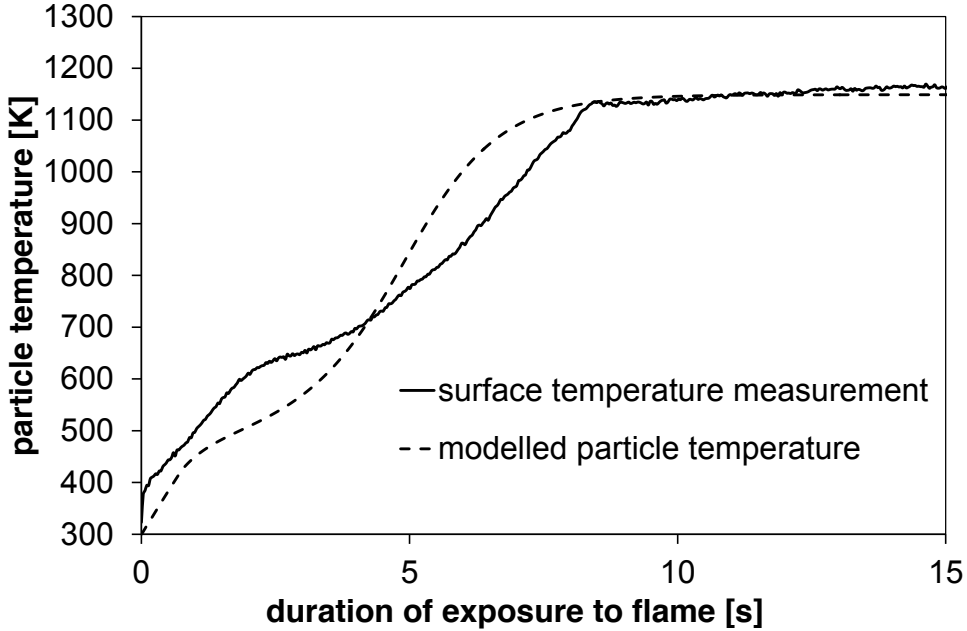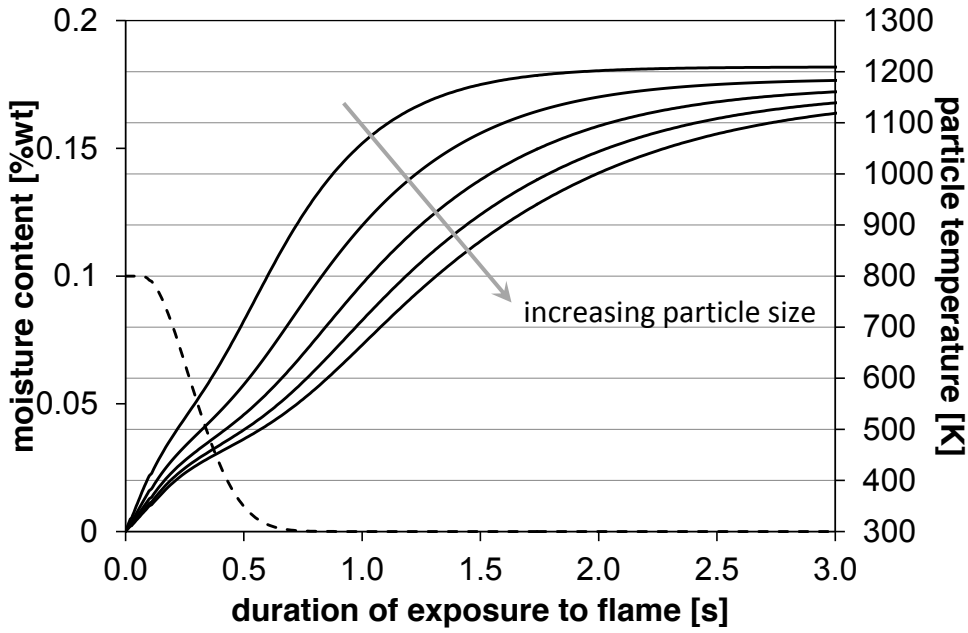
Figure 5 - (a) modelled 300K to 500K heat-up time for 3%, 20% and 50% moisture content; (b) modelled ignition delay for 3% and 50% fitted to data for willow

Fig 5A
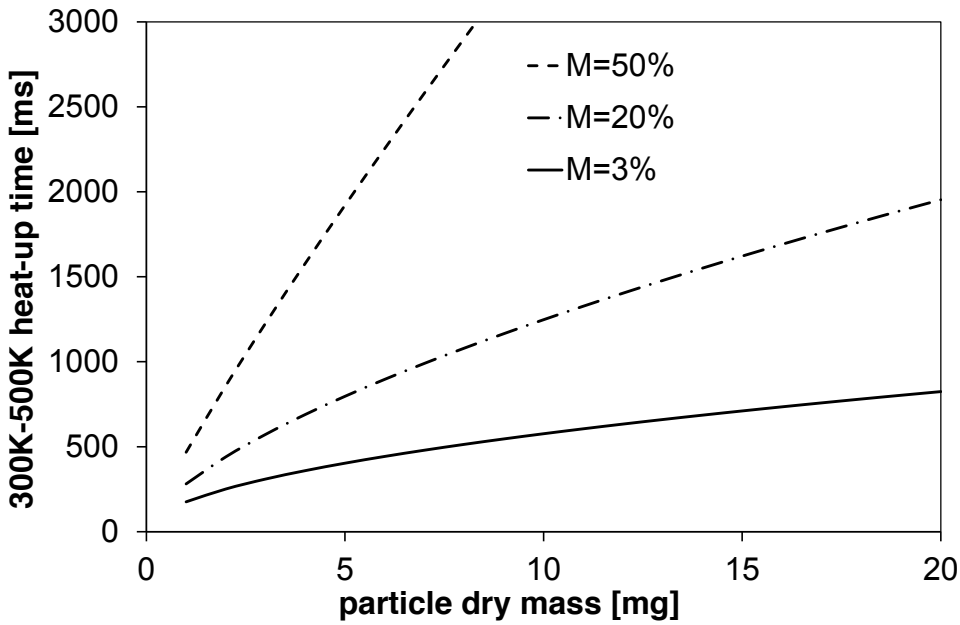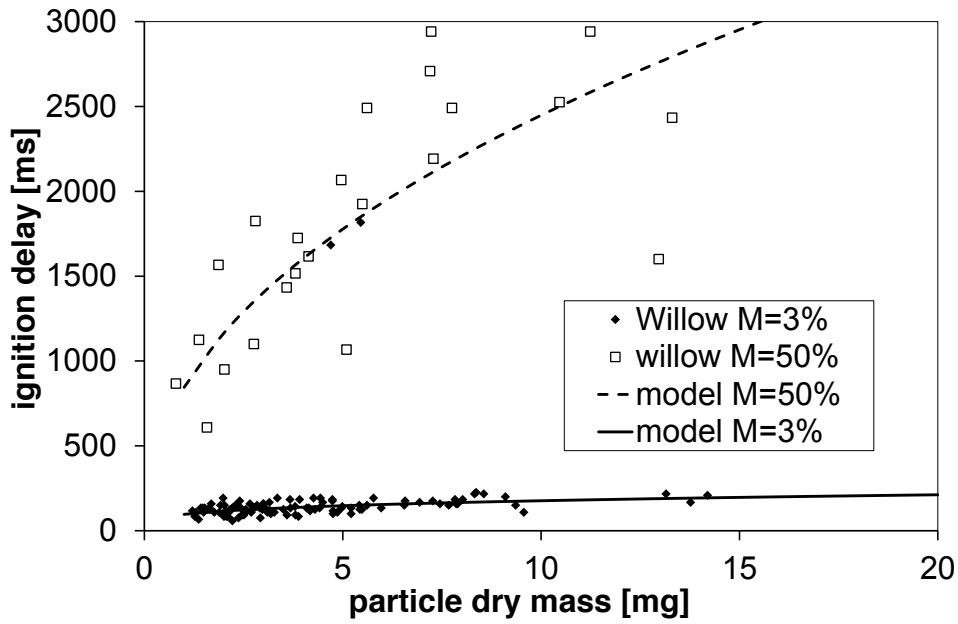
Figure 6 - (a) modelled devolatilisation for particles with increasing size; (b) devolatilisation times versus particle mass: modelled with FG-Biomass; modelled with simplified one-step reaction; best-fit function to volatile flame duration data for pine.
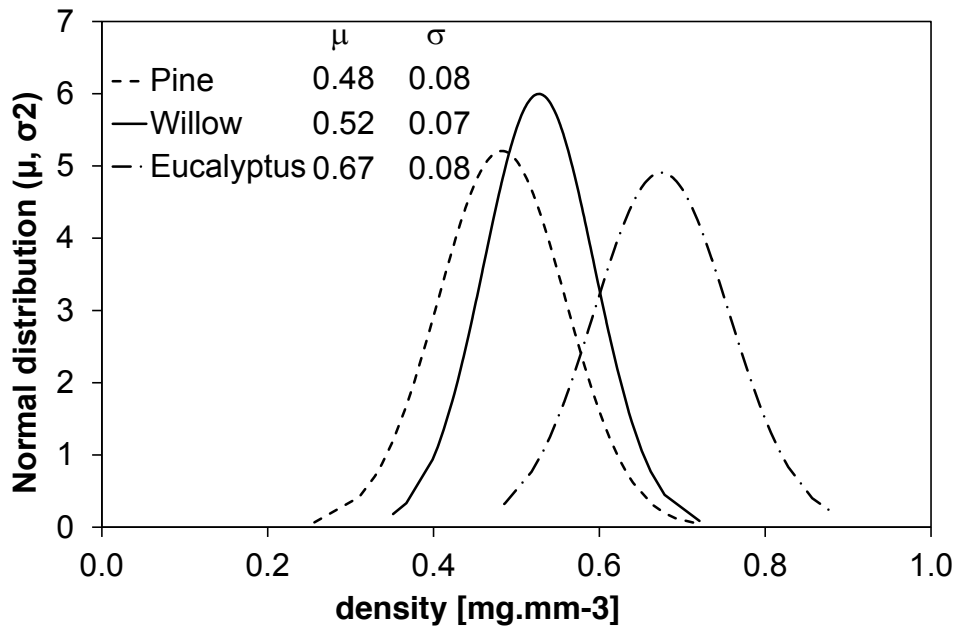
Fig 6A
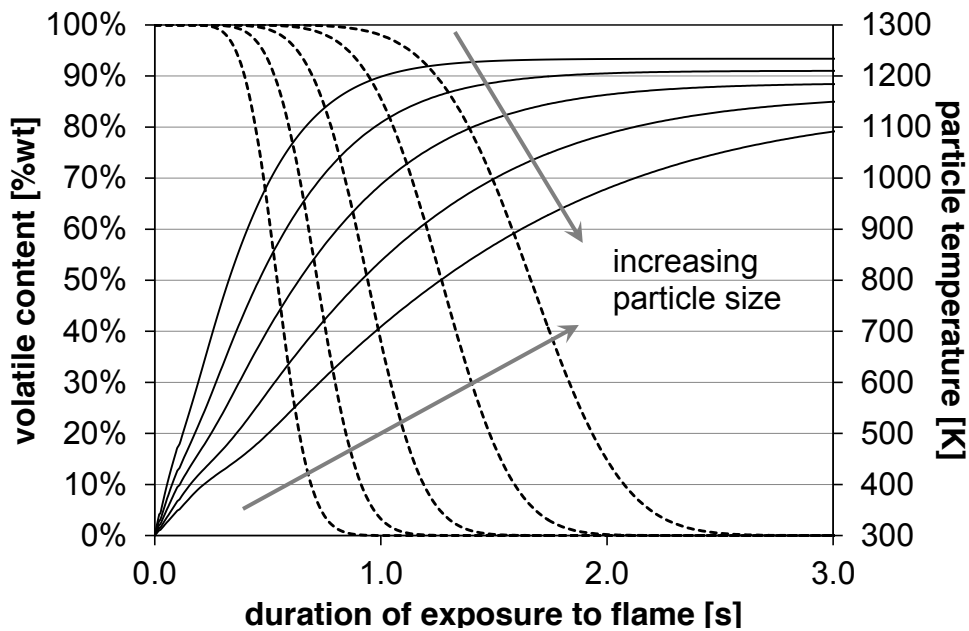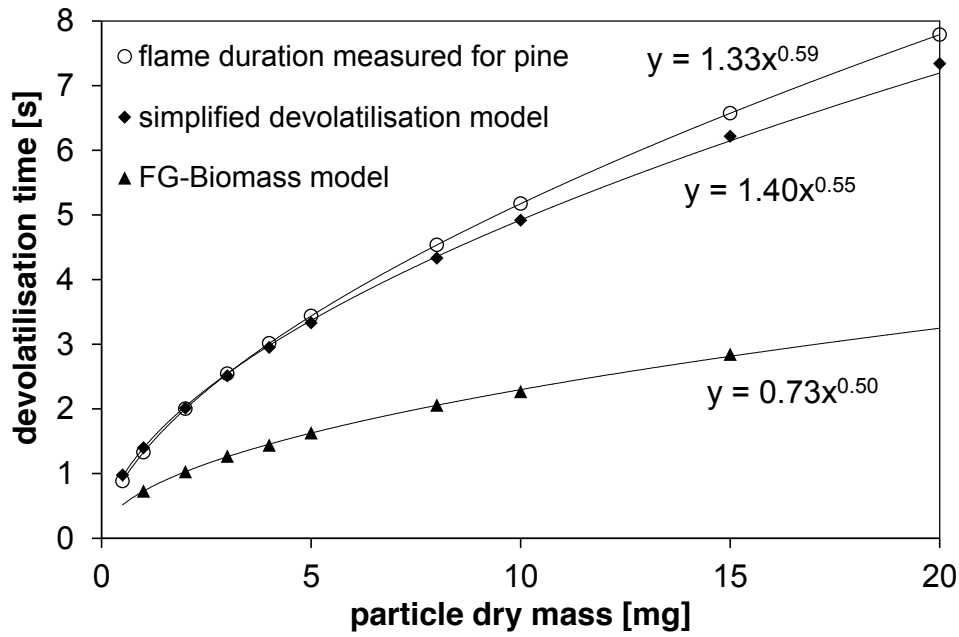
Figure 7 – Particle density distributions for pine; willow; eucalyptus.

Fig 7

Figure 8 – Experimental data for pine separated into 3 density fractions for: (a) volatile flame duration versus particle dry mass; (b) char burn duration versus particle dry mass
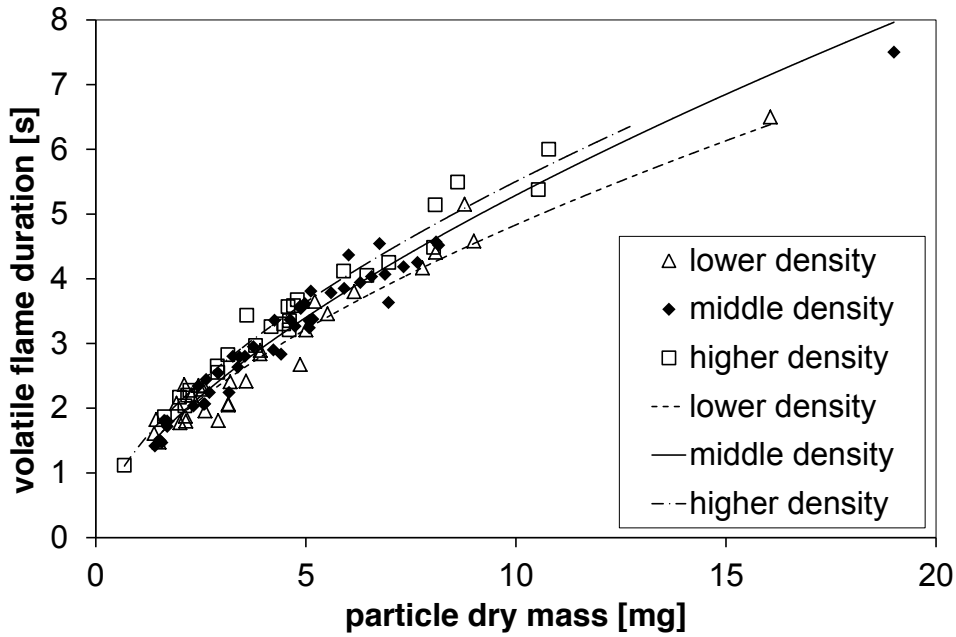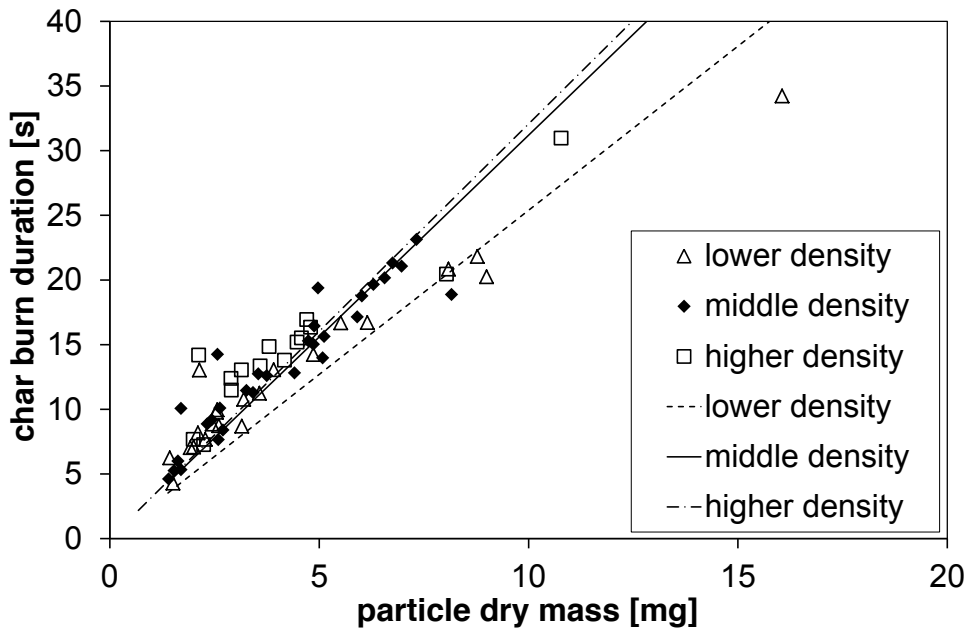
Fig 8A

Fig 8B

Figure 9 - volatile flame duration versus particle dry mass for: (a) 4 shape types – all samples; (b) 4 aspect ratio ranges for willow
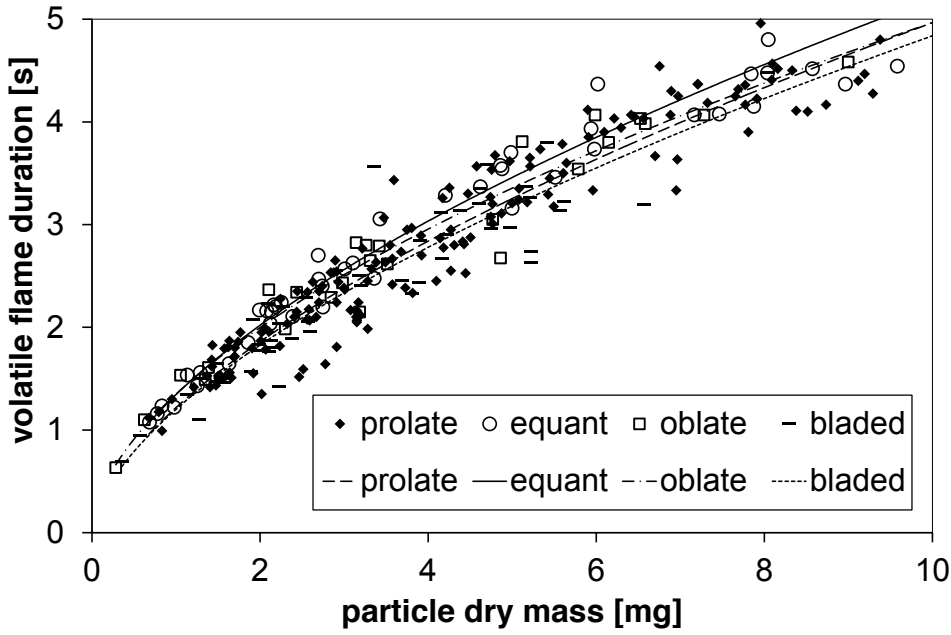
Fig 9A

Fig 9B